DOI: 10.1002/((please add manuscript number))
Article type: Communication

Tailored Transition Metal-doped Nickel Phosphide Nanoparticles for Electrochemical Oxygen Evolution Reaction (OER)

Ho-Wing Man, Chui-Shan Tsang, Molly Meng-Jung Li, Jiaying Mo, Bolong Huang, Lawrence Yoon Suk Lee, Thomas Yun-chung Leung, Kwok-Yin Wong, and Shik Chi Edman Tsang

H.-W. Man, Dr. C.-S. Tsang, Dr. B. Huang, Dr. L. Y. S. Lee, Prof. T.YC Leung, Prof. K.-Y. Wong, Prof. S.C.E. Tsang (visiting)
Department of Applied Biology and Chemical Technology and the State Key Laboratory of Chirosciences, The Hong Kong Polytechnic University, Hung Hom, Kowloon, Hong Kong

Dr. M. M-J. Li, J. Mo, Prof. S. C. E. Tsang
Department of Chemistry, University of Oxford, Oxford, OX1 3QR, UK.

Corresponding e-mails: lawrence.ys.lee@polyu.edu.hk and edman.tsang@chem.ox.ac.uk

Keywords: metal doping, nickel phosphide, electrocatalysis, oxygen evolution reaction

Foreign transition metals are doped into the hexagonal nickel phosphide structure by simple and facile bottom-up wet-chemical synthesis via stabilization with oleylamine, trioctylphosphine (TOP), and trioctylphosphine oxide (TOPO). The as-prepared transition metal-doped nickel phosphide nanoparticles show a high level of doping but creating no significant distortion of crystal structure and morphology against pristine nickel phosphide nanoparticle. Iron-doped nickel phosphide nanoparticle is found to exhibit excellent activity on electrochemical oxygen evolution reaction (OER), having overpotential as small as 330 mV at 20 mA cm^{-2} with a low Tafel slope value of 39 mV dec^{-1}. The result discloses a novel tunable optimization in electron filling and band position of NiP by Fe, which also offers a synergetic surface effect between Ni and Fe to reduce activation barrier for the OER.

Water splitting provides an attractive pathway to produce renewable and sustainable energy sources, which is close to economic breakeven.[1] Hydrogen and oxygen gases are produced by water reduction and oxidation, respectively. Product gases, hydrogen and oxygen,

are collected separately for further use in different sectors in society. Electrochemical oxygen evolution reaction (OER) is worthwhile being studied as another half reaction to complete the entire cycle in alkaline water electrolysis or water splitting reaction.[1]

Electrochemical OER is a multistep reaction where oxygen gas can be formed by the oxidation of water molecules and hydroxide ions in acidic and alkaline media, respectively. OER involves transfer of four electrons which leads to sluggish kinetics and requires high overpotential. The benchmark OER electrocatalysts are conductive ruthenium dioxide (RuO_2) and iridium dioxide (IrO_2).[2] These two oxide materials provide low overpotential which makes them suitable to be OER electrocatalysts. However, their scarcity and high cost make them unfavorable for future commercial uses. With the pioneering works on RuO_2 and IrO_2, other classes of materials, including metal alloys, transition metal oxides, nitrides and phosphides have recently been explored as the new classes of potential OER electrocatalysts, especially for the development of robust and economic competitive transition metal oxide OER electrocatalysts.[1-3] Various classes of oxygen-containing materials including perovskites,[4] spinel family,[5] and layered double hydroxides[6] are being investigated for their potency to carry out the electrochemical OER for dioxygen production.

In general, most transition metal oxides give high impedance due to their insulating or semiconductive properties which hamper the materials from use as electrodes. In contrast, thin layer of transition metal oxide can be utilized for OER on alloy substrate or conductive surface such as carbon nanotube to give the desirable low impedance. Nevertheless, the distribution of metals on these structures cannot be well controlled since many times, local metal segregation as core-shells, ensembles or islands of one metal to another may be created. Thus, this may introduce complex and non-tailoring effects in hybrid systems.[1,2]

Recently, metallic nature of nickel phosphide nanoparticle and doped nanoparticles has been found to be active for both HER and OER reactions. Surface skin of nickel phosphide is in situ converted into the catalytically-active nickel oxyhydroxide species which shows good

activity towards electrochemical OER.[6] This may have opened a new era on employing transition metal modification to the nickel phosphides as rational OER electrocatalysts although no systematic studies are yet carried out.[1,6] With simple modification of the material by metal doping, metal-doped nickel phosphide (NiMP) nanoparticles may show tunable energy levels and electron filling of their resulting electronic band structure to give rise to different surface synergetic chemistry as well as optimized catalytic activities toward electrochemical OER. However, one key challenge is to identify a good synthesis method to substitute Ni with transition metals homogeneously. Herein, various transition metal-doped nickel phosphide nanoparticles are prepared as NiMP in hcp structure without much structural distortion by a template-free bottom-up wet-chemistry method via mixed solvents stabilization (see Figures S1-S6, Table S1). Both theoretical and practical measurements indicate that the typical NiFeP phase clearly remains to be in metallic form (Figures. S7- S8) and EXAFS indicates a near homogeneous substitution of Ni by Fe at 1:1 level without significant distortion of the coordination environment (Figures. S9-S11, Tables S2 and S3). These doped composite materials are investigated for electrocatalytic activity on OER in alkaline medium.

Pristine and metal-doped nickel phosphide nanoparticles were coated on glassy carbon electrode and their linear sweep voltammograms (LSVs) were obtained from 1.2 to 1.8 V (*vs.* RHE, unless stated otherwise) in 1 M potassium hydroxide aqueous solution (**Figure 1a**). The overpotential of pristine nickel phosphide (Ni_2P) nanoparticle at 20 mA cm^{-2} was determined to be 0.39 V. The as-synthesized NiMP nanoparticles (where M = Co, Fe, Mn, and Mo) showed different changes in activity towards electrochemical OER. Overpotential of NiCoP, NiMnP, and NiMoP nanoparticles at 20 mA cm^{-2} are determined to be 0.41, 0.55, and 0.43 V, respectively, which are higher than that of Ni_2P nanoparticle. NiFeP nanoparticle shows an exceptional promising activity than Ni_2P nanoparticle towards electrochemical OER, having an overpotential of as low as 0.33 V at 20 mA cm^{-2}. Despite the different effects of metal doping on OER activity, Ni_2P and all the NiMP nanoparticles exhibited low overpotentials to drive

OER electrochemically which are comparable to the benchmark OER conductive electrocatalysts (RuO_2 and IrO_2). In addition to low overpotential for Ni_2P and NiMP, the corresponding average Tafel slopes were obtained from the polarization plots of Ni_2P and various NiMP nanoparticles (**Figure 1b)**. Ni_2P nanoparticle has a Tafel slope of 58 mV dec^{-1}. Interestingly, the Tafel slope of NiFeP nanoparticle is 39 mV dec^{-1} which is significantly smaller than Ni_2P nanoparticle and even slightly lower than that of RuO_2 and IrO_2 (approximately 40 mV dec^{-1}).[1] This change in Tafel slope suggests the incorporation of iron altered favorably the kinetics of electrochemical OER of the composite. In contrast, NiCoP, NiMnP, and NiMoP nanoparticles show the higher Tafel slopes of 52, 63, and 86 mV dec^{-1}, respectively. Based on the comparisons of overpotentials and Tafel slopes among samples tested, NiFeP nanoparticle showed the most potential as a new OER electrocatalyst (Table S3). The reaction order of hydroxide ion in the NiFeP nanoparticle-catalyzed electrochemical OER was determined by carrying out cyclic voltammetry in potassium hydroxide solution of different concentrations (0.1 to 1 M). A plot of current densities at 0.6 V (low applied voltage) vs. SCE against concentration of KOH solution in logarithmic scale is obtained to estimate reaction order of hydroxide ion (Figure S12). The slope is estimated to be 0.98 indicating that the reaction order of hydroxide ion is close to unity in the rate determining step.

Transition metal M as metallic doper or as electron ligand can alter the band position and its electron filling of the metallic Ni_2P phase hence affecting the resulting OER activity.[7] By plotting average activity (current density) versus contributed d electron (both s and d electrons) of different transition metals (**Figure 2a**), it is clearly evident that Fe of group 8 gives the proper balanced electron filling to antibonding and bonding bands of modified Ni_2P, giving the optimal bonding interaction with M-O required for OER catalytic cycle as guided by theoretical calculations.[7] Interestingly, the anticipated less or greater degree of electrons donation of specific transition metals to the bands of NiP fall in the predicted positions from either sides of the volcano, which depicts a rational approach to alter the electronic structure of this composite

for OER. A small discrepancy is the use of second row transition metal, Mo where the energy of 4d and its ligand overlap are markedly different from that of the 3d transition metals. Notice that inverse average Tafel slopes also match with measured activities over different electron fillings. We have discounted any major contribution from isomorphic or lattice distortion (strain effect) since the transition metal is almost homogeneous substituted to the Ni position.[7] We also note that from Figure 1 that the specific activity and Tafel slope do not give the same values but dependent on the applied voltage. The specific activity shows some degree of correlation with fundamental M-O bond strength of transition metal.[8] Using low applied potential of 1.5 V where the higher concentration of OH^- and lower positive charged electrode (low activity), the activity is actually dependent on the M-O bonding formation as a principle rate determining step hence the stronger nature of M-O such as Fe gives excellent activity compared to other transition metals (Figure S13a). Thus, the exposed Fe on surface of the composite NiFeP with strong Fe-O bond will favor adsorption of OH^- with unit order as described in Figure S12. Conversely, using higher applied potential of 1.8 V where the depleting concentration of OH^- and higher positive charged electrode (high activity) the specific activity becomes to favor more dominated of M-O bond cleavage hence the weaker nature of M-O such as Ni and Co give comparable activity to Fe (Figure S13b). Thus, there is an apparent synergetic effect for both exposed transition metal atoms on the surface of NiFeP composite to work cooperatively: the formation of oxyhydroxide may be mainly taken place on surface Fe to form Fe-O and then Ni catalyzes cleavage of Ni-O bond for O_2 formation to complete the OER catalytic cycle, probably in redox way in transferring surface species. Thus, the proposed elementary mechanism for NiFeP nanoparticle follows reported oxyhydroxide-mediated mechanism that involve both M-O bond and M-O cleavage routes, see **Figure 2b**.[9-12] Hence, NiFeP with unique tunable conductive band structure and homogeneous surface composition can give excellent OER activity.

In addition, electrochemical impedance spectroscopy (EIS) was carried out for both Ni_2P and NiFeP nanoparticle to investigate the effect of Fe doping on the overall conductivity of the composite. The equivalent circuit was constructed to compose of three components, which represent electrolyte, in situ formed surface oxide layer, and phosphide layer underneath.[9] The semicircle in Nyquist plot clearly reveals the small degree of charge transfer resistance for both materials indicative of their bulk metallic nature. Nyquist plot of NiFeP nanoparticle gives even a smaller semicircle than that of Ni_2P nanoparticle which indicates a lower charge transfer resistance in NiFeP nanoparticle (fast redox) than in Ni_2P nanoparticle (**Figure 3a**).

Stability is an essential criterion for development of OER electrocatalyst. Therefore, the best OER electrocatalyst, NiFeP nanoparticle, is also subjected to test for stability. Oxygen evolution reaction was carried out with the applied potential held at 1.47 V in 1 M KOH for 4 h (**Figure 3b**). The current density of approximately 2 mA cm^{-2} was maintained for 4 h indicating NiFeP nanoparticle is a stable electrocatalyst for OER.

In summary, we report a facile chemical synthesis and performance of pristine and metal-doped nickel phosphide nanoparticles as electrocatalysts for OER. Metallic iron-doped nickel phosphide nanoparticle at controllable level with tunable electron bands and filling offers an excellent electrocatalytic activity with an overpotential of as low as 330 mV at 20 mA cm^{-2} and a low Tafel slope of 39 mV dec^{-1}, indicative a comparable if not superior activity to RuO_2 and IrO_2. Surface transition metal with strong M-O formation is formed prior to the oxygen evolution at low potential while M-O bond cleavage plays a crucial role in OER evolution at higher potential. A homogeneous fast redox couple of Fe and Ni on the same metallic hcp phosphide structure thus offers high rate for adsorption of hydroxides, deprotonation and M-O cleavage and transfer of species to form oxygen molecules on surface in a catalytic cycle. It is for the first time demonstrated that such conductive but stable phosphide phase to host and disperse metal atoms can provide tunable synergetic catalytic properties for efficient OER.

Experimental Section

Synthesis of pristine and metal-doped nickel phosphide nanoparticles. Typically, phosphide nanoparticles were prepared by decomposition of soluble metal precursor(s) and phosphorus source in the presence of capping ligands and solvents as bottom up synthesis. The total number of moles of metal ions was kept as 1 mmol in preparing both pristine and metal-doped nickel phosphide nanoparticles. Table S1 showed detailed amount of metal precursor(s) used in preparation of each sample. The metal precursor was dissolved in 5 mL oleylamine and put under vacuum to remove adventitious oxygen and moisture. 11.2 mmol of trioctylphosphine (TOP) and equimolar of trioctylphosphine oxide (TOPO) were added to the flask sequentially and was heated at 300 °C for 2 h under N_2. After 2 h, the reaction mixture was cooled down naturally by removal of heat source. 30 mL absolute ethanol was added, and precipitate was collected by centrifugation at 9000 rpm for 5 min. Supernatant was discarded and precipitate was purified by redispersion/precipitation process using chloroform and ethanol. The process was repeated for three times and purified product was dried and kept under vacuum.

Characterization. Powdered X-Ray diffraction pattern was obtained using Rigaku SmartLab with scan rate of 1° min^{-1}. Powdered sample was placed on a silicon wafer and pressed using a glass slide. Diffraction pattern from $2\theta = 35°$ to 60° was obtained for pristine and various metal-doped nickel phosphide nanoparticles. As-prepared powder samples were dispersed and sonicated in chloroform to obtain well-dispersed suspension. 20-40 μL of suspension was added on a 400-mesh copper grid with holely carbon coating and dried naturally. Images from transmission electron microscopy were obtained using a scanning transmission electron microscope (JOEL JEM-2100F). Selected area electron diffraction (SAED) and energy-dispersive X-ray spectroscopy (EDX) were carried out in tandem in transmission electron microscopy. Approximately 20 mg of powder sample was used in analysis. X-Ray photoelectron spectra of pristine and various metal-doped nickel phosphide nanoparticles were obtained using X-Ray photoelectron spectrophotometer (ESCALAB 250 Xi). Calibration was done using binding energy of C 1s energy level at 284.8 eV as reference.

Preparation of working electrode. Catalyst ink was prepared by dissolving 2.5 mg metal-doped nickel phosphide nanoparticles in a solution containing 460 µL ethanol-water mixture (3:7) and 40 µL 5 wt.% Nafion solution. Working electrode was prepared by drop-casting 10 µL of catalyst ink on glassy carbon electrode (GCE, d = 3 mm, surface area = 0.0707 cm^2). The catalyst ink was dried naturally.

Measurement of performance on electrochemical OER. Electrochemical measurements were performed using a CHI potentiostat (CHI1030A). Electrocatalytic oxygen evolution reaction was conducted in a typical three-electrode system, using Pt mesh and saturated calomel electrode (SCE) as the counter and reference electrode, respectively, in 1 M potassium hydroxide solution (pH = 14). The electrolyte solution was purged with Ar for 30 min before the electrochemical measurements to get rid of dissolved oxygen and provide inert atmosphere. Linear sweep voltammetry (LSV) was carried out in a potential range of 0.13 and 0.19 V with a scan rate of 5 mV/s. The potentials measurement against saturated calomel electrode (SCE) were converted with respect to the reverse hydrogen electrode (RHE) according to the following equation:[13]

$$E_{RHE} = E_{SCE} + 0.244 + 0.0592(pH)$$

Electrochemical impedance spectroscopy. Electrochemical impedance spectroscopy (EIS) was carried out in 1 M KOH aqueous solution that was purged with Ar prior to measurement. Graphite rod and SCE were used as the counter and reference electrodes, respectively. The EIS was measured in the frequency range of 10 mHz and 1 MHz with an amplitude of 5 mV.

Estimation of reaction order of hydroxide ion. Cyclic voltammetry was carried out from -0.1 V to 1 V *vs.* SCE under KOH solution with concentration of 0.1, 0.25, 0.5 and 1 M. Current density at 0.6 V *vs.* SCE was plotted against hydroxide ion concentration in logarithmic scale. The slope of the plot was equivalent to reaction order of hydroxide ion according to the following equation:[14]

$$m = \frac{\partial \ln j}{\partial \ln [OH^-]}$$

where m is the reaction order of hydroxide ion, and j is the current density at potential at 0.6 V *vs.* SCE.

Stability test for electrochemical OER. The working electrode coated with NiFeP nanoparticles was tested for the stability by holding the potential at 1.47 V *vs.* RHE for 4 h.

Supporting Information
Supporting Information is available from the Wiley Online Library or from the author.

Acknowledgements
We thank B18 of Diamond light source, UK to provide access to XAS analysis of the materials.

Received: ((will be filled in by the editorial staff))
Revised: ((will be filled in by the editorial staff))
Published online: ((will be filled in by the editorial staff))

References

[1] N-T. Suen,S-F. Hung,Q. Quan, N. Zhang, Y-J. Xu and H. M. Chen, Chem. Soc. Rev. **2017**, *46*, 337.

[2] a) R. Frydendal, E. A. Paoli, B. P. Knudsen, B. Wickman, P. Malacrida, I. E. L. Stephens, I. Chorkendorff, ChemElectroChem **2014**, *1*, 2075; b) Y. Lee, J. Suntivich, K. J. May, E. E. Perry, Y. Shao-Horn, J. Phys. Chem. Lett. **2012**, *3*, 399.

[3] S. Gottesfeld, S. Srinivasan, J. Electroanal. Chem. Interfacial Electrochem. **1978**, *86*, 89.

[4] a) J. O. M. Bockris, T. Otagawa, J. Electrochem. Soc., **1984**, *131*, 290; b) A. Grimaud, K. J. May, C. E. Carlton, Y.-L. Lee, M. Risch, W. T. Hong, J. Zhou, Y. Shao-Horn, Nat. Commun. **2013**, *4*, 2439; c) J. G. Lee, J. Hwang, H. J. Hwang, O. S. Jeon, J. Jang, O. Kwon, Y. Lee, B. Han, Y.-G. Shul, J. Am. Chem. Soc. **2016**, *138*, 3541.

[5] a) I. Nikolov, R. Darkaoui, E. Zhecheva, R. Stoyanova, N. Dimitrov, T. Vitanov, J. Electroanal. Chem. **1997**, *429*, 157; b) Y. Li, P. Hasin, Y. Wu, Adv. Mater. **2010**, *22*, 1926; c) F. Cheng, J. Shen, B. Peng, Y. Pan, Z. Tao, J. Chen, Nat. Chem. **2011**, *3*, 79; d) T. Maiyalagan, K. A. Jarvis, S. Therese, P. J. Ferreira, A. Manthiram, Nat. Commun. **2014**, *5*, 3949.

[6] a) M. Gong, Y. Li, H. Wang, Y. Liang, J. Z. Wu, J. Zhou, J. Wang, T. Regier, F. Wei, H. Dai, J. Am. Chem. Soc. **2013**, *135*, 8452; b) Z. Lu, W. Xu, W. Zhu, Q. Yang, X. Lei, J. Liu, Y. Li, X. Sun, X. Duan, Chem. Commun. **2014**, *50*, 6479; c) F. Song, X. Hu, Nat. Commun. **2014**, *5*, 4477; d) F. Song, X. Hu, J. Am. Chem. Soc. **2014**, *136*, 16481; e) H. Liang, F. Meng, M. Cabán-Acevedo, L. Li, A. Forticaux, L. Xiu, Z. Wang, S. Jin, Nano Lett. **2015**, *15*, 1421; f) Z. Pu, C. Zhang, I. S. Amiinu, W. Li, L. Wu, S. Mu, ACS Appl. Mater. Interfaces **2017**, *9*, 16187.

[7] a) G. Młynarek, M. Paszkiewicz, A. J. Radniecka, J. Appl. Electrochem. **1984**, *14*, 145.; b) D. A. Corrigan, J. Electrochem. Soc. **1987**, *134*, 377.; c) E. L. Miller, R. E. Rocheleau, J. Electrochem. Soc. **1997**, *144*, 3072.; d) X. Li, F. C. Walsh, D. Pletcher, Phys. Chem. Chem. Phys. **2010**, *13*, 1162; e) M. Gong, Y. Li, H. Wang, Y. Liang, J. Z. Wu, J. Zhou, J. Wang, T. Regier, F. Wei, H. Dai, J. Am. Chem. Soc. **2013**, *135*, 8452.

[8] J. D. Cox, D. D. Wagman, V. A. Medvedev. Eds., CODATA Key Values for Thermodynamics, Hemisphere Publishing Corporation, New York, **1989**.

[9] a) B. W. Zhang, Y. H. Lui, L. Zhou, X. H. Tang, S. Hu, J. Mater. Chem. A **2017**, *5*, 13329; b) M. W. Louie, A. T. Bell, J. Am. Chem. Soc. **2013**, *135*, 12329.

[10] R. L. Doyle, I. J. Godwin, M. P. Brandon, M. E. G. Lyons, Phys. Chem. Chem. Phys. **2013**, *15*, 13737.

[11] L. Trotochaud, S. L. Young, J. K. Ranney, S. W. Boettcher, J. Am. Chem. Soc. **2014**, *136*, 6744.

[12] a) J. A. Bau, E. J. Luber, J. M. Buriak, ACS Appl. Mater. Interfaces **2015**, *7*, 19755; b) N. Han, F. Zhao, Y. Li, J. Mater. Chem. A **2015**, *3*, 16348; c) J. Qi, W. Zhang, R. Xiang, K. Liu, H.-Y. Wang, M. Chen, Y. Han, R. Cao, Adv. Sci. **2015**, *2*, 1500199.

[13] F. Lyu, Y. Bai, Q. Wang, L. Wang, X. Zhang, Y. Yin, Dalton Trans. **2017**, *46*, 10545.

[14] M. E. G. Lyons, M. P. Brandon, Int. J. Electrochem. Sci. **2008**, *3*, 1386.

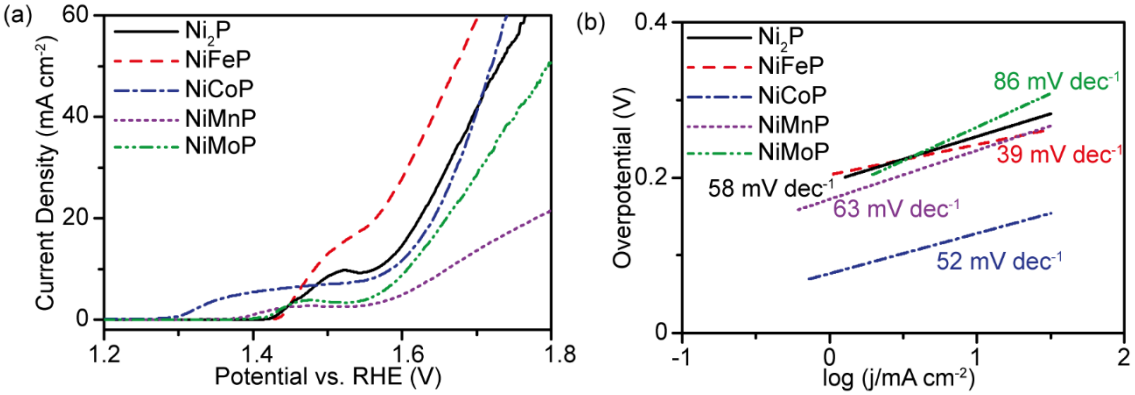

Figure 1. (a) Linear sweep voltammograms and (b) Tafel plots of Ni_2P and NiMP nanoparticles with various Tafel slopes evaluated at about 20 mA cm^{-2} region (low activity region) in 1 M KOH.

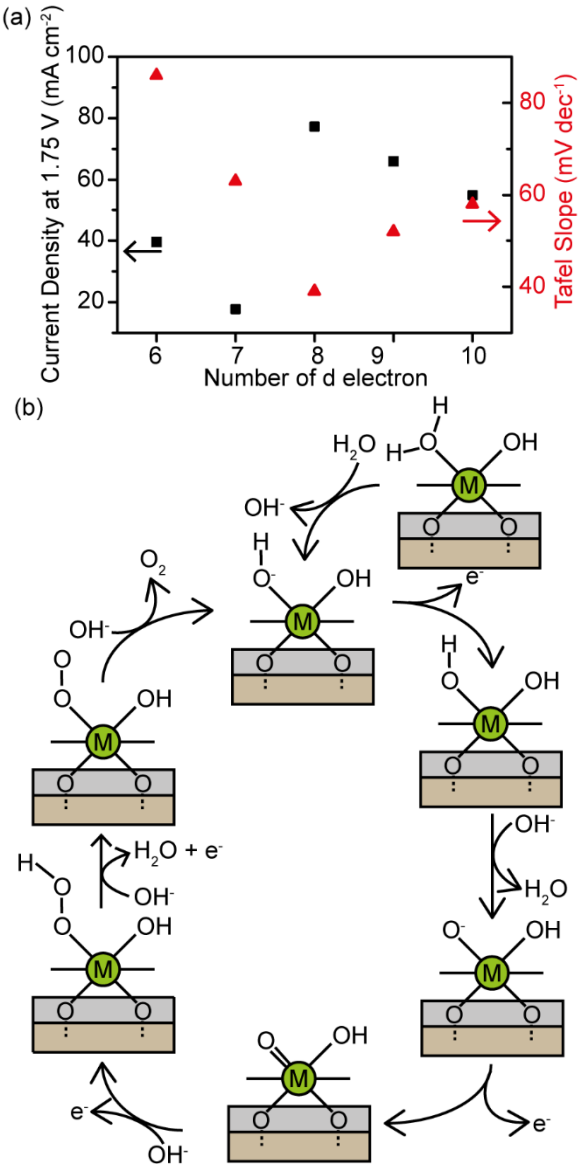

Figure 2. (a) A plot of activity (current density) of NiMP versus total injected d electrons of transition metal M (Mo= 6, Mn= 7, Fe= 8, Co= 9 and Ni= 10) into the NiP bands (the slight

higher activity of Mo with only 6 d-electrons contribution than expected is due to higher energy and more effective 4-d bands overlap with O than that of 3-d bands in other transition metals and (b) Schematic diagram of proposed mechanism for M-O bond formation and M-O bond cleavage on surface M (i.e. Ni and Fe) for electrochemical OER.[8-12]

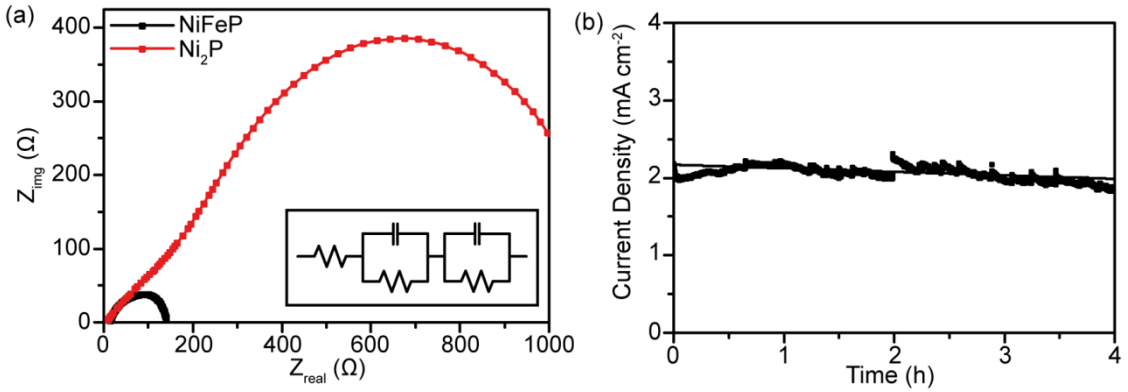

Figure 3. (a) Nyquist plots obtained from electrochemical impedance spectroscopy of iron-doped and pristine nickel phosphide nanoparticles recorded in 1 M KOH solution. Inset showed the equivalent circuit model and (b) Stability test of NiFeP nanoparticle at an applied potential of 1.47 V for 4 h.

The table of contents entry should be 50−60 words long, and the first phrase should be bold.

Iron-doped nickel phosphide nanoparticle is found to exhibit excellent activity on electrochemical oxygen evolution reaction (OER), having over-potential as small as 330 mV at 20 mA cm^{-2} with a low Tafel slope value of 39 mV dec^{-1}. The result discloses a novel tunable optimization in electron filling and band position of NiP by Fe, which also offers a synergetic surface effect between Ni and Fe to reduce activation barrier for the OER reaction.

Keyword: metal doping, nickel phosphide, electrocatalysis, oxygen evolution reaction

Ho-Wing Man, Chui-Shan Tsang, Molly Meng-Jung Li, Jiaying Mo, Bolong Huang, Lawrence Yoon Suk Lee, Kwok-Yin Wong, and Shik Chi Edman Tsang

Title: **Tailored Transition Metal-doped Nickel Phosphide Nanoparticles for Electrochemical Oxygen Evolution Reaction (OER)**

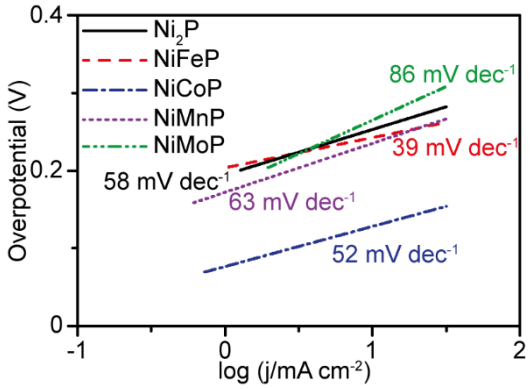

Supporting Information

Transition Metal-doped Nickel Phosphide Nanoparticles for Electrochemcial Oxygen Evolution Reaction (OER)

Ho-Wing Man, Chui-Shan Tsang, Molly Meng-Jung Li, Jiaying Mo, Bolong Huang, Lawrence Yoon Suk Lee, Thomas Yun-Chung Leung, Kwok-Yin Wong, and Shik Chi Edman Tsang

Iron-doped nickel phosphide (NiFeP) nanoparticle was first synthesized to investigate the feasibility of metal doping in nickel phosphide crystal lattice. Nickel and iron metal salts were mixed in the presence of oleylamine, trioctylphosphine (TOP), and trioctylphosphine oxide (TOPO).

X-Ray diffraction (XRD) pattern of NiFeP nanoparticles is shown below (Figure S1). The as-synthesized NiFeP nanoparticle has almost identical diffraction pattern as hcp phase of Ni_2P which consist four peaks at 2θ = 40.7°, 44.7°, 47.4°, and 54.4°. Thus, this diffraction pattern resembles closely to Ni_2P hexagonal crystal structure (PDF#-65-1989) without much peak distortion or peak shift at the high level of Fe doping although line broadening due to small sizes may have prevented accurate peaks comparison. The former three peaks from XRD pattern of NiFeP at 2θ = 40.7°, 44.7°, and 47.4° are corresponding to (111), (201), and (210) lattice planes, respectively. Meanwhile, the two peaks at 54.2° and 55° in Ni_2P reference pattern, corresponding to (300) and (211) lattice planes, respectively, merge together to have a broad peak at 54.4° in XRD pattern of NiFeP nanoparticle due to small crystalline size in nanoparticles.

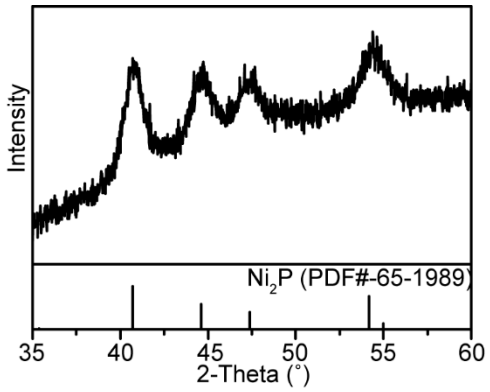

Figure S1. XRD pattern of NiFeP nanoparticle.

Detailed morphology and elemental composition of NiFeP nanoparticle are investigated by transmission electron microscopy (TEM) and energy dispersive X-ray spectroscopy (EDX) equipped in TEM. The TEM image shows the as-synthesized NiFeP nanoparticle is monodispersed and spherical with an average diameter of 7.5 ± 0.9 nm (Figure S2 (a) and (b)). The small size of nanoparticle is coherent with the large full width at half maximum (broad peaks) and small crystalline size in XRD pattern. TEM image taken under high resolution is shown in Figure S2 (c). The predominant (111) lattice fringe shows a *d*-spacing of 0.22 nm. The selected area electron diffraction (SAED) pattern shows the rings of diffraction (Figure S2 (d)), where the innermost ring is indexed as (111) lattice plane and the outermost ring corresponds to (300) lattice plane. The measurement of *d*-spacing and electron diffraction pattern is in good agreements with XRD pattern mentioned previously. The elemental composition is determined by EDX (Figure S3). The normalized ratio of elements in NiFeP nanoparticle (nickel-to-iron-to-phosphorus) is 1:0.1:0.7. An overall 6% of iron is successfully doped into the nickel phosphide crystal lattice.

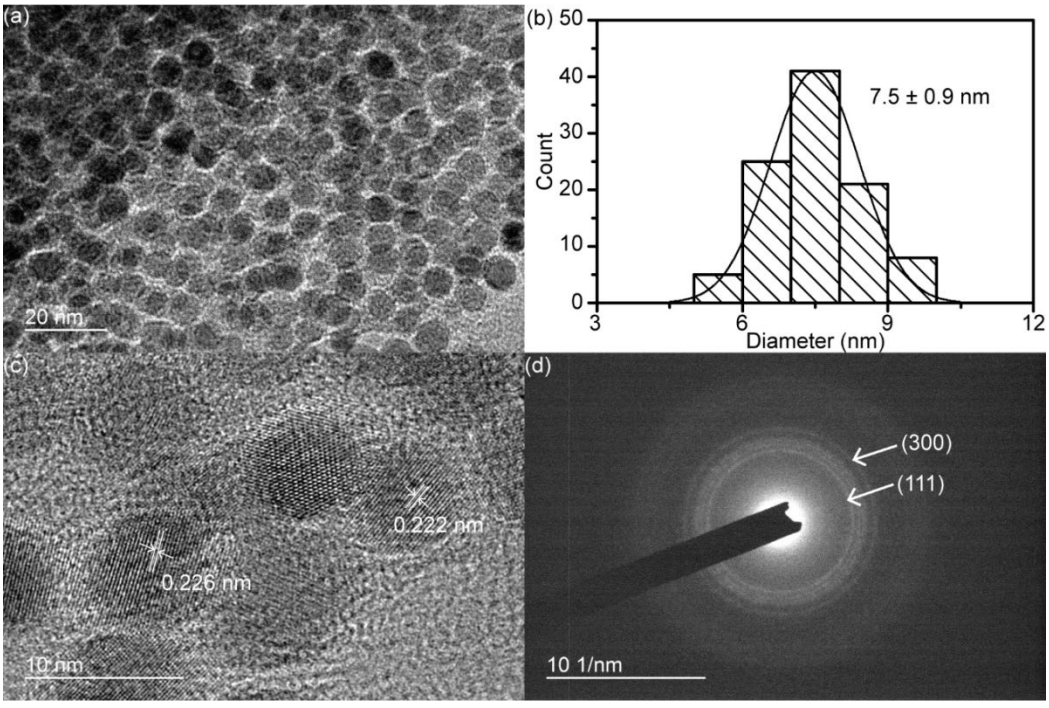

Figure S2. (a) TEM image, (b) and its size distribution, (c) high resolution TEM image, and (d) electron diffraction pattern of NiFeP nanoparticles.

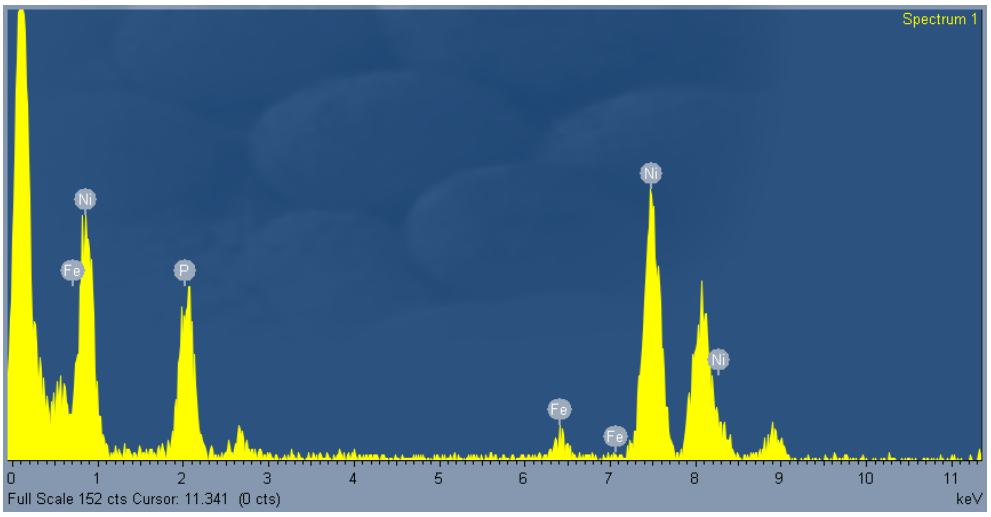

Figure S3. EDX spectrum of NiFeP nanoparticles.

The scope of metal doping is extended to other transition metal ions including cobalt, manganese, and molybdenum ions at high 1:1 doping as NiMP. As a result, other transition metal acetate is used instead of iron(II) acetate as a precursor in synthesis to prepare other transition metal-doped nickel phosphides (NiMP) nanoparticles. The corresponding XRD patterns (Figure S4), TEM images (Figure S5) and composition (Table S1) of NiMP nanoparticles all resemble closely to the Ni_2P reference (PDF#-65-1989, Figure S4) without much peak shift/distortion despite the large extent of transition metal incorporation.

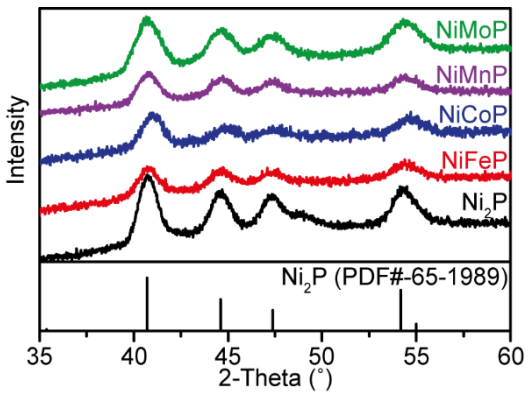

Figure S4. XRD patterns of Ni_2P and various NiMP nanoparticles.

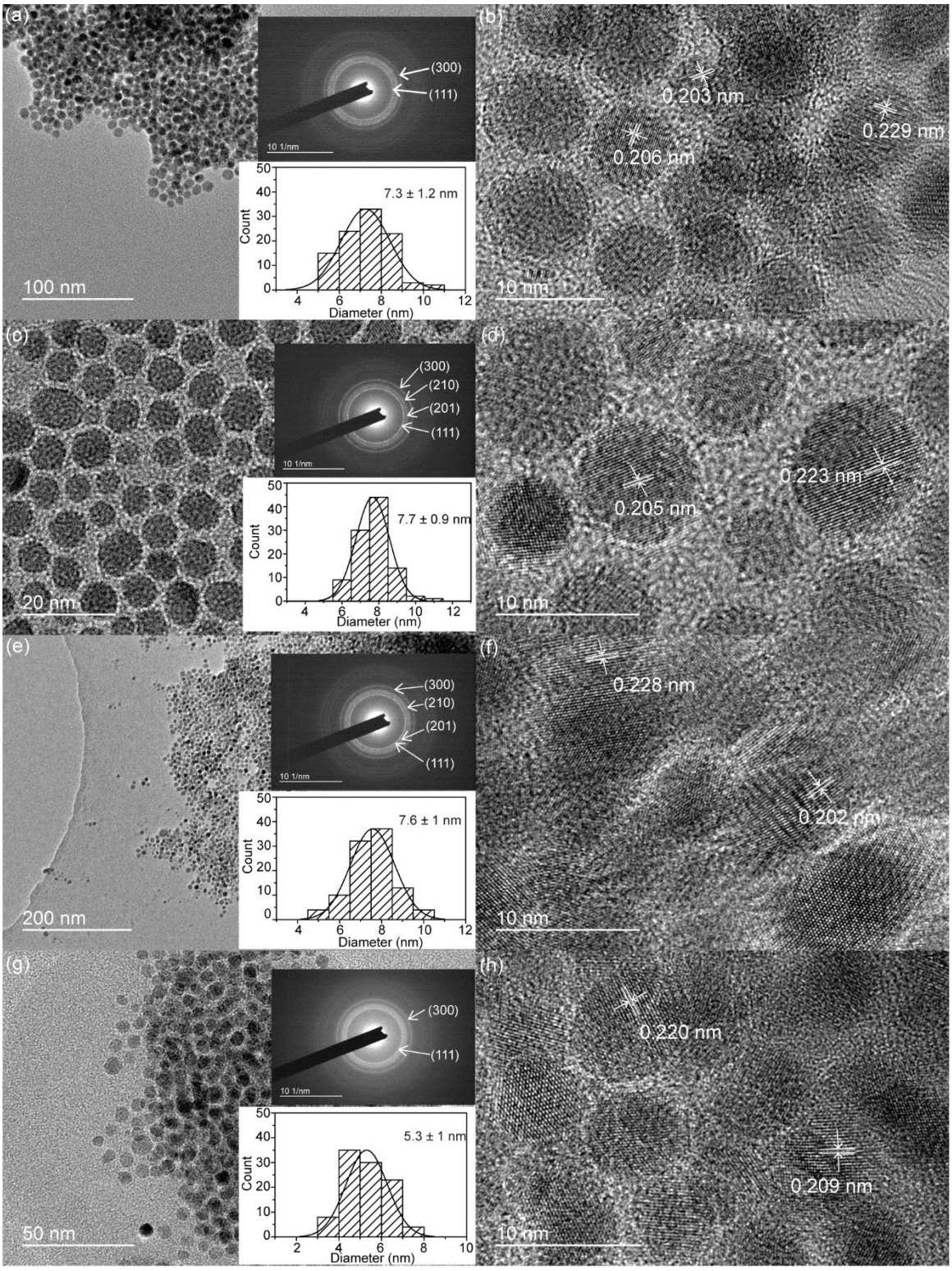

Figure S5. TEM and HR-TEM images with selected area electron diffraction pattern and size distribution in inset. (a and b) Ni_2P, (c and d) NiCoP, (e and f) NiMnP, (g and h) NiMoP nanoparticles showing same morphology and homogeneous doping with comparable lattice fringes observed.

Table S1a. Metal precursor loading for synthesis of pristine and metal-doped nickel phosphide nanoparticles.

	Metal precursor(s)
Ni_2P	$Ni(OAc)_2 \cdot 4H_2O$ (1 mmol)
NiFeP	$Ni(OAc)_2 \cdot 4H_2O$ (0.5 mmol) + $Fe(OAc)_2$ (0.5 mmol)
NiCoP	$Ni(OAc)_2 \cdot 4H_2O$ (0.5 mmol) + $Co(OAc)_2$ (0.5 mmol)
NiMnP	$Ni(OAc)_2 \cdot 4H_2O$ (0.5 mmol) + $Mn(OAc)_3 \cdot 2H_2O$ (0.5 mmol)
NiMoP	$Ni(OAc)_2 \cdot 4H_2O$ (0.5 mmol) + $[Mo(OAc)_2]_2$ (0.25 mmol)

Table S1b. Normalized elemental composition of pristine and metal-doped nickel phosphide nanoparticles by EDX

	Ni	M	P
Ni_2P	2	-	1
NiFeP	1	0.1	0.7
NiCoP	1	0.55	1.2
NiMnP	1	0.05	0.7
NiMoP	1.6	0.08	1

XPS spectra of NiFeP nanoparticle in Ni 2p and P 2p regions also have the peaks similar to typical nickel phosphides (Figure S6a and c).[1] Peaks at 853.0 eV correspond to nickel in nickel-phosphorus bond in Ni $2p_{3/2}$ level. The binding energy is close to zero-valent nickel (852.8 eV)[2] which indicates nickel in nickel-phosphorus bond only bear a small positive charge ($Ni^{\delta+}$).[3] The peaks at 856.1 and 861.5 eV are assigned to the oxidized nickel species (NiO) and its satellite peak in Ni $2p_{3/2}$ level, respectively. Similarly, the peaks at 869.9, 874.1, and 880.1 eV correspond to nickel in nickel-phosphorus bond, oxidized Ni species, and its satellite peak in the Ni $2p_{1/2}$ energy level. In XPS spectrum of P 2p region, the peak at 129.4 eV originates from the phosphorus in nickel-phosphorus bond, while the peak at 133.1 eV corresponds to the surface oxidized phosphorus species such as phosphate. The binding energy of phosphorus in phosphide slightly deviates from elemental phosphorus (130.2 eV) which shows phosphorus in nickel-phosphorus bond bears a small negative charge ($P^{\delta-}$).[4] In addition, the embedded peak at 130.4 eV can be assigned to the phosphorus in iron phosphide domain.[5] For Fe 2p XPS spectrum, the peaks at 711.8 and 713.5 eV correspond to the surface oxidized iron in iron oxide and phosphate in Fe $2p_{3/2}$ energy level, respectively, meanwhile the peaks at 723.5 and 727.9 eV are the counterpart peaks in Fe $2p_{1/2}$ energy level.[6] The peaks at 706.8 and 719.5 can be assigned to the iron in iron phosphide in Fe $2p_{3/2}$ and $2p_{1/2}$ energy level, respectively (Figure S6b).

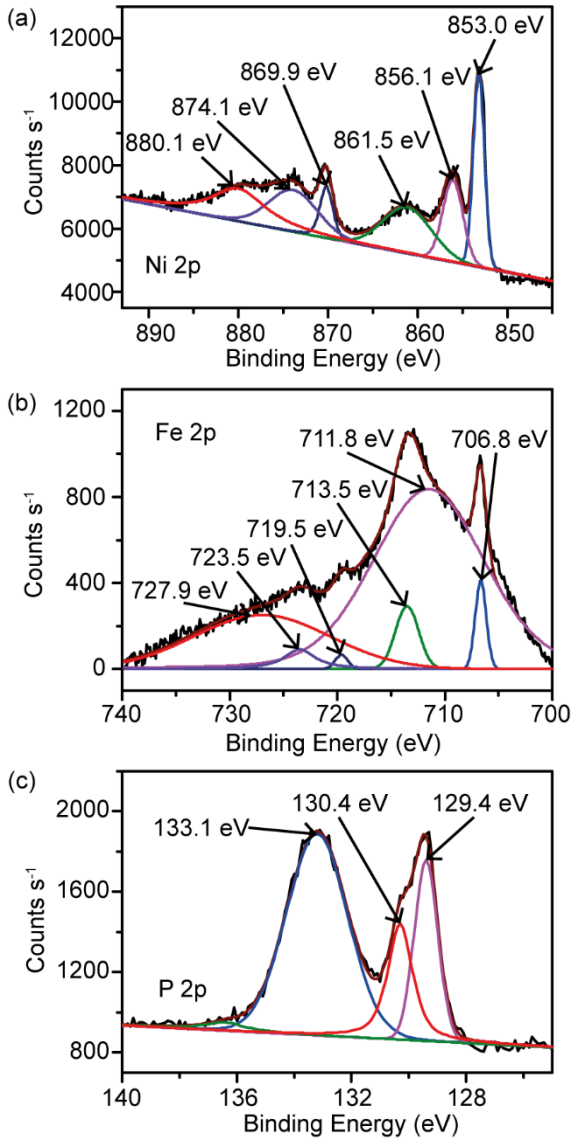

Figure S6. XPS spectra of NiFeP nanoparticle in (a) Ni 2p, (b) Fe 2p, and (c) P 2p.

Ni_xP_y structure

According to the experimental XRD data NixPy resembles to the wurtzite structure of ZnO. As a result, 3D lattice as the prototype host matrix to represent the NiP structure is attempted. The Ni is placed in the position of Zn site and the P is placed in the O site. After the geometrical lattice relaxation under the zero external hydrostatic pressure, the ground state structure of the NixPy follows the symmetry group of *P63/mmc* with structural formula of Ni_2P_2. Figure S7 demonstrates the predicted crystal structure lattice arrangement for this Ni_xP_y. The reciprocal path for the band structure calculations is from Γ (0, 0, 0) to the H (0, 0, ½). The total density

of states (TDOSs) plot shows the strong *p-d* coupled orbital level across the Fermi level (E_F) by Ni-P hybridized bonding.

In the band structure of the BZ, it shows an isotropic metallic behavior indicating a good electronic conductor for charge transfer without barrier. The H point gives a gap up to about 5 eV, denoting the electronic transfer cannot be easily attributed to the path along the Ni-P bonding direction in the real space. There might be another possible mechanism e.g. Coulomb tunneling for charge transfer. Meanwhile, it also means the electronic transport in such conductor is mostly along the direction perpendicular to the plane (i.e. along z-axis) instead of transferring along the in-plane Ni-P bonding direction.

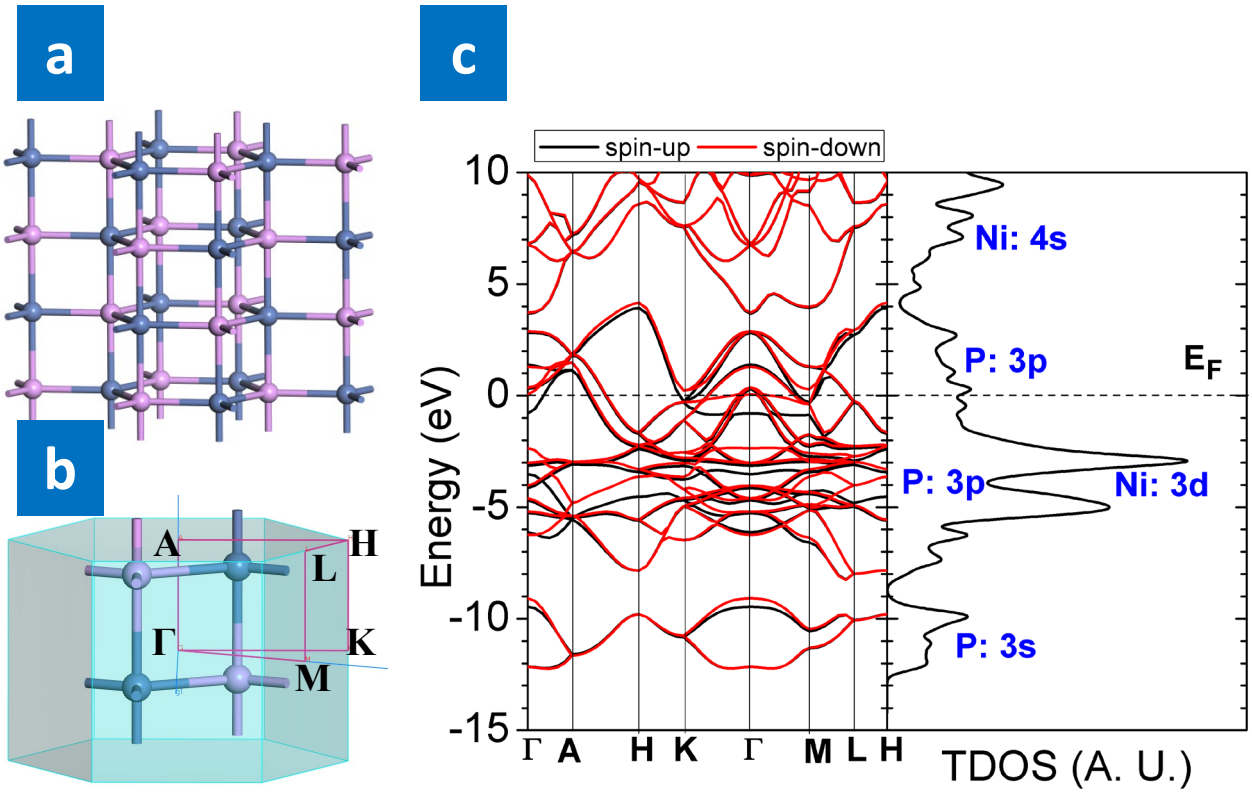

Figure S7. (a) The predicted Ni_2P_2 crystal structure. (b) The related unit cell lattice with reciprocal Brillouin Zone (BZ) presented. (c) The right panel is the electronic band structure and total density of states (TDOSs) along the path formed by the high symmetrical points in the BZ. (Ni=grey, and P=purple).

Metallic structure

Ultra-violet photoelectron spectroscopy (UPS) is carried out for NiFeP nanoparticle to determine the energy of valence band maximum against Fermi level (Figure S8). The energy difference between Fermi level (E_F) and valence band maximum (E_{VBM}) can be found from the interception on abscissa by extrapolating the right-side slope of the peak. The energy difference is estimated as -0.37 eV that implies a higher energy of valence band maximum (VBM) than Fermi level and confirms NiFeP nanoparticle possesses a metallic property.

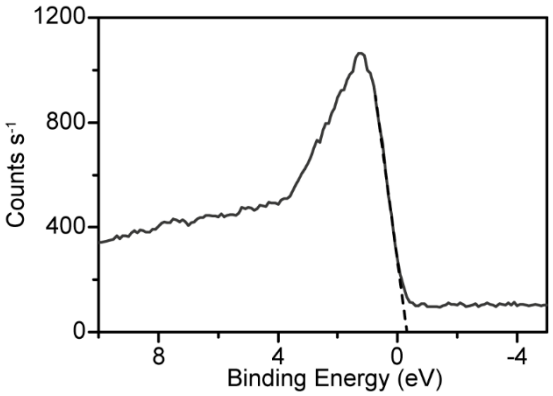

Figure S8. UPS spectrum of NiFeP nanoparticle.

EXAFS studies

Based on the structural analyses of NiFeP and Ni_2P nanoparticles, NiFeP nanoparticle is proved to be synthesized without a significant change in nickel phosphide crystal structure. However, it is difficult to determine the exact localized bonding environments of iron in the crystal lattice by the aforementioned characterizations. In order to have further information on the structure, the extended X-ray absorption fine structure (EXAFS) measurement is carried out. It measures the average coordination number of surface atoms and estimates bond lengths, and thus helps getting a better picture on the bonding environment and local structure of each element in NiFeP nanoparticle. The data for NiFeP nanoparticle were recorded and the fittings were carried out with satisfaction (Figure S10, Figure S11, and Table S3), which depicted the

hcp structure (Figure S7). The bond lengths of various combinations of elements are estimated, including nickel-phosphorus (Ni-P), nickel-nickel (Ni-Ni), iron-nickel (Fe-Ni), and iron-phosphorus (Fe-P) bonds. Ni-Ni and Ni-P bonds are 2.59 and 2.24 Å, respectively. Meanwhile, Fe-Ni and Fe-P bonds are 2.63 and 2.21 Å, respectively. The EXAFS data confirmed the existence of iron incorporation in nickel phosphide and iron is bonded to both nickel and phosphorus in the hcp crystal lattice as illustrated in Figure S7. The fitted data from EXAFS measurement of Ni_2P nanoparticle show the Ni-Ni and Ni-P bond lengths in Ni_2P nanoparticle are 2.59 and 2.25 Å, respectively (Figure S9 and Table S2). The bond lengths in iron-doped and pristine nickel phosphide nanoparticle are comparable which shows the incorporation of iron in nickel phosphide crystal lattice do not induce significant changes in bond strengths of existing Ni-Ni and Ni-P bonds. Typical coordination numbers in Ni-Ni and Ni-P for Ni_2P are 4 and 2, respectively, which are close to the fittings shown in Table S2, having coordination numbers for Ni-Ni and Ni-P as 3.3 and 2.9, respectively.[7] There is, however, a decrease in the coordination numbers when Fe is introduced into the crystal lattice. The coordination numbers for Ni-Ni and Ni-P in NiFeP nanoparticles are 2.5 and 2.3, respectively, whereas those for Fe-Ni and Fe-P are determined to be 3.6 and 3.7, respectively. The decreased coordination numbers of Ni-Ni and Ni-P indicate successful substitution of Ni with Fe. In addition, the change in coordination number does not reveal a perfect substitution since there is a degree of mismatch between the added coordination numbers of Ni-P and Fe-P in NiFeP nanoparticle and that of Ni-P in Ni_2P nanoparticle. But, the basic hcp structure is clearly maintained.

From the above control experiments for NiFeP nanoparticle synthesis, it was confirmed that iron present in the reaction environment can be incorporated into nickel phosphide crystal lattice without making much significant effect on the morphology, crystal structure, and bonding environment of the resulting nanoparticles despite the large degree of Fe incorporation.

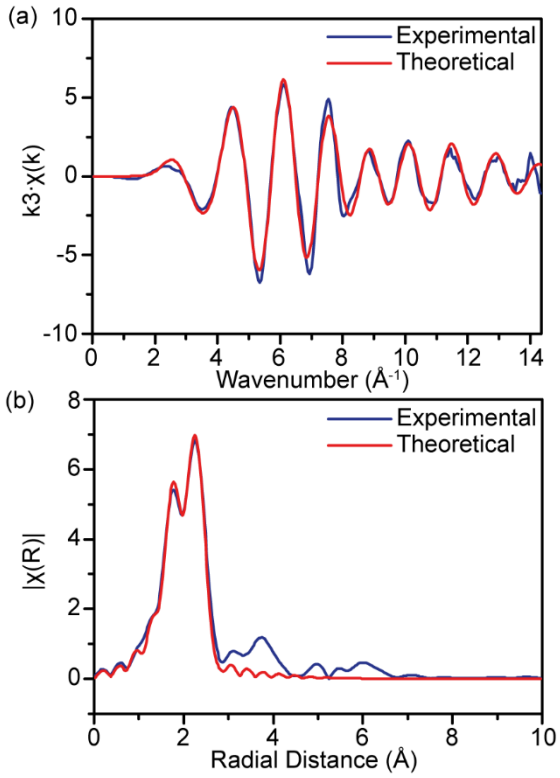

Figure S9. EXAFS plots of (a) $k^3 \cdot \chi$ of experimental and fitted data and (b) $k^3 \cdot \chi$ phase corrected Fourier transform of experimental and fitted data for Ni_2P nanoparticle with Ni K-edge transmission mode.

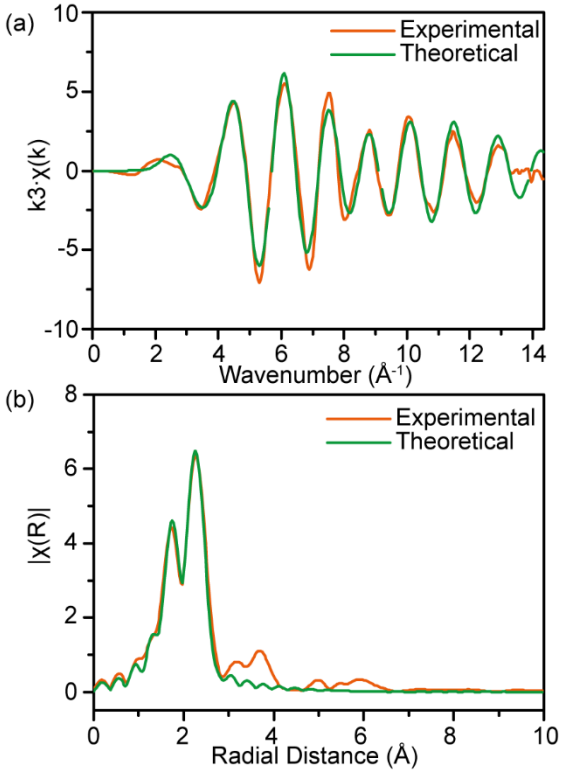

Figure S10. EXAFS plots of (a) $k^3 \cdot \chi$ of experimental and fitted data and (b) $k^3 \cdot \chi$ phase corrected Fourier transform of experimental and fitted data for NiFeP nanoparticle with Ni K-edge transmission mode.

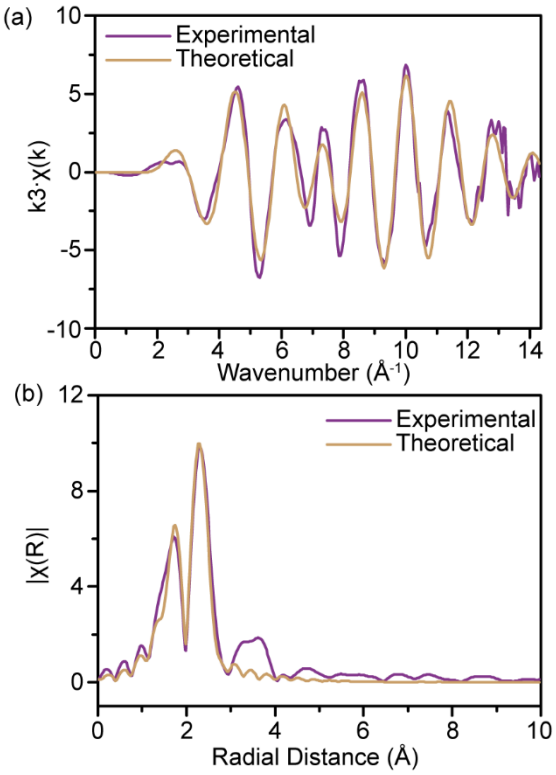

Figure S11. EXAFS plots of (a) $k^3 \cdot \chi$ experimental and fitted data and (b) $k^3 \cdot \chi$ phase corrected Fourier transform of experimental and fitted data for NiFeP nanoparticle with Fe K-edge transmission mode.

Table S2. EXAFS of Ni_2P nanoparticle.

Bond	Enot*	Coordination number	Ss	Bond length (Å)	R-factor
Ni-P	2.7	2.9(2)	0.008(1)	2.25(1)	0.6%
Ni-Ni		3.3(3)	0.008(1)	2.59(1)	

*Enot is the energy different of absorption energy in experimental value and calculated value.

Table S3 EXAFS of NiFeP nanoparticle.

Bond	Enot*	Coordination number	Ss	Bond length (Å)	R-factor
Ni-P	4.3	2.3(3)	0.008(2)	2.24(1)	1.3%
Ni-Ni		2.5(3)	0.006(1)	2.59(1)	
Fe-P	5.5	3.7(3)	0.007(1)	2.21(1)	2.0%
Fe-Ni		3.6(3)	0.005(1)	2.63(1)	

*Enot is the energy difference of absorption energy in experimental value and calculated value.

The above EXAFS experiments were carried out in B18 Diamond light source. Si(111) Double Crystal Monochromator (DCM) was used to scan the photon energy. The energy resolution ($\Delta E/E$) for the incident X-ray photons was estimated to be 2×10^{-4}. Transmission mode was adopted for Ni K-edge and Fe K-edge EXAFS measurements. To ascertain the reproducibility of the experimental data, at least two scan sets were collected and compared for each sample. The EXAFS data analysis was performed using IFEFFIT 1 with Horae packages 2 (Athena and Artemes). The spectra were calibrated with Ni and Fe metal foils as the references to avoid energy shifts of the samples. The amplitude reduction factors were obtained from EXAFS data analysis of the references, which were used as the fixed input parameters in the data fitting to allow the refinement in the coordination number of the absorption element. In this work, the first shell data analyses under the assumption of single scattering were performed with the errors estimated by R-factor.

Table S4. Summary of electrochemical parameters of pristine and various metal-doped nickel phosphide nanoparticles.

	Overpotential at 20 mA cm^{-2} (V)	Tafel slope (mV dec^{-1})
Ni_2P	0.39	58
NiFeP	0.33	39
NiCoP	0.41	52
NiMnP	0.55	63
NiMoP	0.43	86

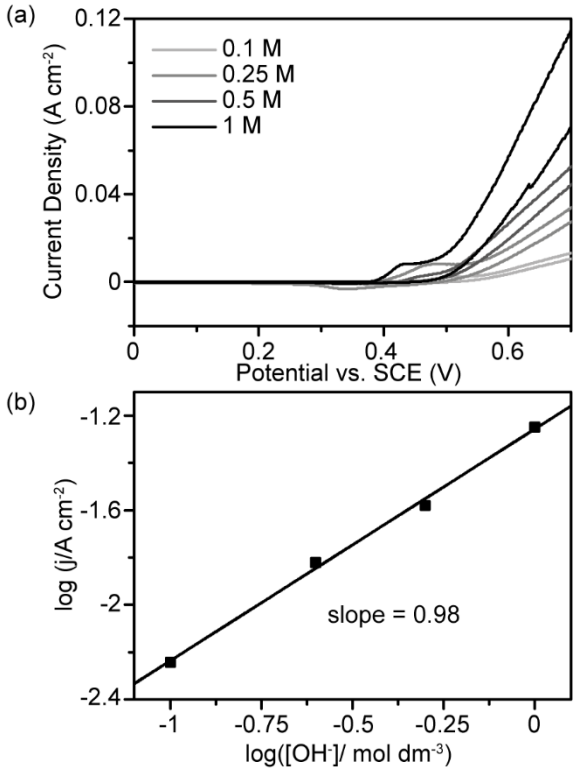

Figure S12. Cyclic voltammograms of NiFeP nanoparticle in KOH solution with different concentrations and (b) relationship between current density at 0.6 V vs. SCE and concentration of hydroxide ion.

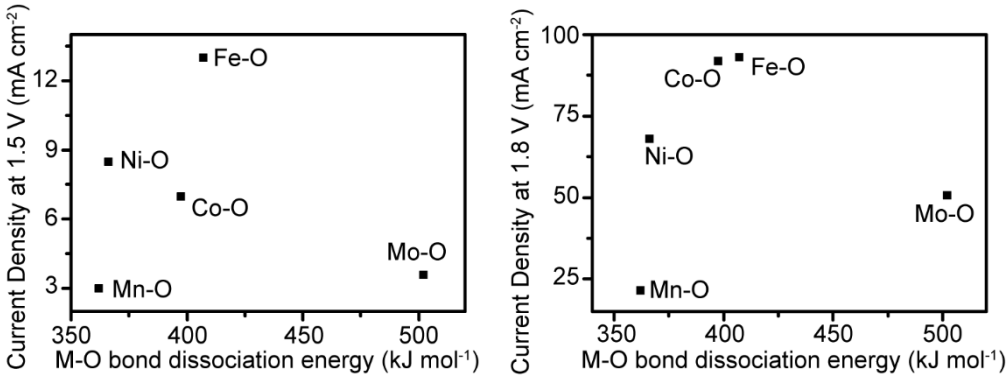

Figure S13. (a) Correlation of the activity (current density) of composite NiMP with M-O bond energy (left) low applied potential of 1.5V where the higher concentration of OH^- and lower positive charged electrode (low activity) favor the M-O bonding formation as a principle rate determining step hence stronger nature of M-O i.e. Fe gives relatively good activity and (b) high applied potential of 1.8V where the depleting concentration of OH^- and higher positive charged electrode (high activity) tends to favor the bond cleavage of M-O hence the weaker nature of M-O i.e. Co, Ni gives relatively high activity with reference to Fe.

Reference

[1] Y. Pan, Y. Liu, J. Zhao, K. Yang, J. Liang, D. Liu, W. Hu, D. Liu, Y. Liu, C. Liu, J. Mater. Chem. A **2015**, *3*, 1656.

[2] A. B. Mandale, S. Badrinarayanan, S. K. Date, A. P. B. Sinha, J. Electron Spectrosc. Relat. Phenom. **1984**, *33*, 61.

[3] Z. Huang, Z. Chen, Z. Chen, C. Lv, H. Meng, C. Zhang, ACS Nano **2014**, *8*, 8121.

[4] a) J. Li, Y. Chai, B. Liu, Y. Wu, X. Li, Z. Tang, Y. Liu, C. Liu, Appl. Catal., A **2014**, *469*, 434; b) Y. Zhao, Y. Zhao, H. Feng, J. Shen, J. Mater. Chem. **2011**, *21*, 8137.

[5] C. E. Myers, H. F. Franzen, J. W. Anderegg, Inorg. Chem. **1985**, *24*, 1822.

[6] a) Y. Yan, B. Y. Xia, X. Ge, Z. Liu, A. Fisher, X. Wang, Chem. - Eur. J. **2015**, *21*, 18062; b) J. Masud, S. Umapathi, N. Ashokaan, M. Nath, J. Mater. Chem. A **2016**, *4*, 9750.

[7] H. R. Seo, K-S. Cho, S-H. Kim, Y-K. Lee, J. Korean Phys. Soc. **2010**, *56*, 2083-2087.